The statistical behaviour of attached eddies

J. D. Woodcock and I. Marusic

Citation: Physics of Fluids **27**, 015104 (2015); doi: 10.1063/1.4905301
View online: http://dx.doi.org/10.1063/1.4905301
View Table of Contents: http://scitation.aip.org/content/aip/journal/pof2/27/1?ver=pdfcov
Published by the AIP Publishing

PHYSICS OF FLUIDS **27**, 015104 (2015)

The statistical behaviour of attached eddies

J. D. Woodcock and I. Marusic
Department of Mechanical Engineering, University of Melbourne, Victoria 3010, Australia

(Received 24 July 2014; accepted 19 December 2014; published online 12 January 2015)

Townsend's attached eddy hypothesis forms the basis of an established model of the logarithmic layer in wall-bounded turbulent flows in which this inertially dominated region is characterised by a hierarchy of geometrically self-similar eddying motions that scale with their distance to the wall. The hypothesis has gained considerable support from high Reynolds number measurements of the second-order moments of the fluctuating velocities. Recently, Meneveau and Marusic ["Generalized logarithmic law for high-order moments in turbulent boundary layers," J. Fluid Mech. **719**, R1 (2013)] presented experimental evidence that all even-ordered moments of the streamwise velocity will exhibit a logarithmic dependence on the distance from the wall. They demonstrated that this was consistent with the attached eddy hypothesis, so long as the velocity distribution is assumed to be Gaussian (which allows the use of the central limit theorem). In this paper, we derive this result from the attached eddy model without assuming a Gaussian velocity distribution, and find that such logarithmic behaviours are valid in the large Reynolds number limit. We also revisit the physical and mathematical basis of the attached eddy hypothesis, in order to increase rigour and minimise the assumptions required to apply the hypothesis. To this end, we have extended the proof of Campbell's theorem to apply to the velocity field corresponding to a forest of variously sized eddies that are randomly placed on the wall. This enables us to derive all moments of the velocity in the logarithmic region, including cross-correlations between different components of the velocity. By contrast, previous studies of the attached eddy hypothesis have considered only the mean velocity and its second order moments. From this, we obtain qualitatively correct skewnesses and flatnesses for the spanwise and wall-normal fluctuations. The issue of the Reynolds number dependence of von Kármán's constant is also addressed. © *2015 AIP Publishing LLC.* [http://dx.doi.org/10.1063/1.4905301]

I. INTRODUCTION

Turbulence has proved to be a notoriously difficult phenomenon for which to produce physical models. This is in large part due to the fact that turbulent flows consist of motions at a multitude of scales, most of which must be accounted for in any successful model. For this reason, the earliest models of turbulence have instead regarded the flow as being subjected to perfectly random fluctuations, with empirically determined average behaviours. This dearth of predictive physical models is a significant ongoing inconvenience in both theoretical and practical applications.

However, we are not entirely without physical models of wall turbulence. In 1961, Townsend postulated that the logarithmic region of turbulent flows along walls could be modelled as a three-dimensional distribution of self-similar eddying motions whose sizes scale with their distance from the wall.[1] This, he reasoned, follows from the fact that the rate of dissipation within the fluid scales with its distance from the wall. The size of each eddy was therefore proportional to its distance from the wall, and in this loose sense, the eddies could be said to be "attached" to the wall. This has come to be known as the attached eddy hypothesis. The great advantage of the attached eddy hypothesis is that it replaces the many scales of swirling motions with a single eddy motion and allows a consideration of the statistics that derive from all three components of velocity. In this

way, the attached eddy model is unique, and provides insights into scaling behaviour for changing Reynolds number, amongst other trends.

Townsend was able to produce physical predictions from the attached eddy model. In order to do so, however, he had adopted a prescribed distribution of eddy sizes that produced a constant Reynolds shear stress.[2] Using this model, Townsend was able to derive the second order moments of the velocity fluctuations. If u, v, and w represent the velocity fluctuations in the streamwise, spanwise, and wall-normal dimensions, respectively, Townsend found that

$$\langle u^2 \rangle^+ = B_1 - A_1 \log\left(\frac{z}{\delta}\right), \tag{1a}$$

$$\langle v^2 \rangle^+ = B_{1,v} - A_{1,v} \log\left(\frac{z}{\delta}\right), \tag{1b}$$

$$\langle w^2 \rangle^+ = B_{1,w}, \tag{1c}$$

where the angled brackets indicate ensemble averages. The superscript + indicates that the quantities have been scaled according to viscous wall-units. The distance from the wall is represented by z, and δ denotes the maximum distance from the wall at which the flow is dominated by the presence of the attached eddies. All of the As and Bs above are constants.

This result only applies where the flow is sufficiently close to the wall to feel its presence, and yet sufficiently distanced that the effect of viscosity is negligible, except at the smallest scales. Therefore, these formulations essentially apply in the inner portion of the inertially dominated region, referred to most commonly as the "log region."

Tellingly, this result contradicted the classical view of wall turbulence, since it implies that the kinetic energy will vary through the log-region. Conversely, the classical view assumed that the kinetic energy would be constant.[3,4]

The nature of the log region, and the coherent structures within it, has been reviewed extensively in recent years by various authors.[5–9] While differing interpretations remain with regard to the causal relationships between the flow features and coherent structures (in particular, vortical structures), a consensus appears to have emerged that the flow in the log region is associated with a hierarchy of eddying motions, which scale with their distance from the wall, in line with Townsend's original hypothesis.[1]

Moreover, experiments at high Reynolds number[10–15] and recent direct numerical simulations[16] report strong support for the logarithmic behaviours for the profiles of the velocity fluctuations, as given in (1).

The attached eddy hypothesis has also been used to derive the flow profile for the mean flow for wall-flows by Perry and Chong[17] and Perry, Henbest, and Chong.[18] In the streamwise direction, they obtained the classical logarithmic law of the wall

$$\langle U \rangle^+ = \frac{1}{\kappa} \log\left(z^+\right) + C, \tag{2}$$

where κ is the von Kármán constant, and C is a parameter that depends on the roughness of the surface and is assumed to be a constant for smooth-walled flows. There has been some debate as to whether κ is truly a constant or is in fact dependent on the Reynolds number.[2,19] This will be investigated in Sec. III B.

Further studies extended the attached eddy hypothesis to include wake effects and streamwise pressure gradients.[20–22] These studies associated the attached eddies with the "wall structure," and the physically detached eddies with the "wake structure." It was found that the presence of both types of eddies is necessary in order to obtain correct quantitative results for all components of the Reynolds stress. (The derivation that will be given in this work disregards the wake region and will therefore be analogous to the derivation by Perry and Marusic[21] with their $T, w = 1$.)

Further refinements of the attached eddy work were carried out by Marusic.[23] This was in order to account for experimental evidence indicating that the streamwise velocity autocorrelation length in the log region extends over several boundary layer thicknesses in length. This was also consistent with the PIV experiments of Adrian *et al.*[24] who reported the tendency of attached-type eddies to align themselves in "packets" in the streamwise direction, rather than being perfectly

randomly and independently positioned. This naturally results in a series of long streamwise streaks of high and low streamwise velocity forming in the log region. Further experimental evidence has been found for the existence of such organised motion by various authors.[25,26] Marusic also showed that using packets of hairpin-type vortices as the representative eddy structure produced results that quantitatively agreed with the autocorrelation statistics.[23] A review of the attached eddy model is also presented by Tardu.[27]

In more recent work, Meneveau and Marusic[28] extended Eq. (1) for the streamwise component to higher order even-numbered moments. However, in order to do so, they had assumed that the velocity distribution is Gaussian. This allows the central limit theorem to be applied to the velocity field. The moments so derived were

$$\left\langle \left(u^+\right)^{2p} \right\rangle^{1/p} = B_p - A_p \log\left(\frac{z}{\delta}\right), \tag{3}$$

where B_p and A_p are constants, and the A_p relates to each other via

$$A_p = [(2p-1)!!]^{1/p}\, A_1, \qquad \text{where } n!! \equiv n(n-2)(n-4)\ldots 1.$$

Furthermore, using high Reynolds number data, they showed that the dependence of high-order even moments on z/δ in the logarithmic layer follows (3), but the prefactors A_p fall below the Gaussian prediction. (Deviations from Gaussian predictions are to be expected since the central limit theorem only strictly applies in the limit as the number of eddies present approaches infinity and when their contributions are assumed to be statistically independent.)

We will subsequently show that the higher order even-numbered moments of the streamwise and spanwise velocity will obey (3), in the asymptotically high Reynolds number limit. We will also show that the wall-normal velocity fluctuations entirely fail to display such Gaussian behaviour.

In this work, we revisit the attached eddy hypothesis and adopt a more rigorous physical and mathematical model for turbulent flows in the log-region than has been done previously. In doing so, we reconsider the physical theory and basic assumptions upon which the attached eddy model is based, and seek to minimize the physical assumptions necessary for deriving the properties of the flow from the model. Furthermore, while previous studies had only derived the first and second order moments, this analysis has made it possible to derive moments of the velocity to any order. The natures of the higher order moments are somewhat counter-intuitive, in that they could not be approximated or guessed by extrapolating the known behaviours of the lowest order moments.

To this end, we utilise Campbell's theorem, which was first applied to the attached eddy hypothesis by Marusic,[23] following the suggestion of Adrian.[41] As in the works of Townsend, Perry and Chong, and others, we model the flow as a random distribution of geometrically similar eddies, whose locations are independent of each other. However, those previous studies have also assumed that the distribution of eddy sizes takes a specific form, chosen for convenience. They have further assumed *a priori* that any combined effects of eddies of differing heights will be negligible. In Sec. II A, we show that the eddy size distribution does in fact follow from simple physical principles. We also subsequently demonstrate mathematically that it is indeed the case that the combined effects of eddies of different sizes do not affect the moments of the velocity.

The model and its assumptions are formulated in Sec. II. A derivation of Campbell's theorem is given in Appendix B. From this, the logarithmic laws and related properties of the flow have been derived in Sec. III.

II. MATHEMATICAL FORMULATION

The model presented here pertains to the log-region and is therefore inertial and inviscid. Viscosity is not considered, except in that it sets the lower bound of the log-region. (In other words, it sets the scale of the smallest attached eddy.) As a result, the standard no-slip boundary conditions cannot be applied. Instead, we apply the method of images. Each eddy is paired with an identical mirror eddy on the other side of the wall. In this way, we guarantee non-penetration of the flow through the wall.

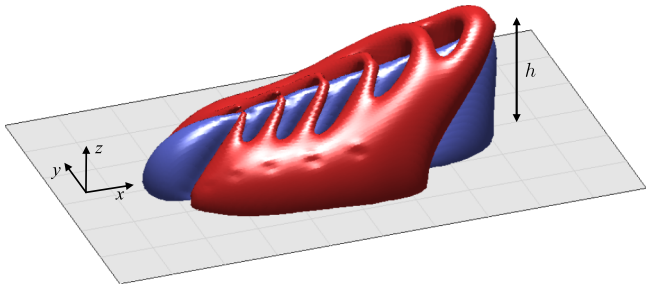

FIG. 1. Sketch of the streamwise velocity field associated with a typical representative eddy. The red and blue regions represent, respectively, isocontours of streamwise velocity in excess of and below the mean velocity. The eddy and its induced velocity field have only one length scale (h).

The model is intended to determine the statistical properties of a statistically steady-state flow, and makes no reference to the dynamics of the flow. However, it is noted that recent studies by Sharma and McKeon[29] and Moarref *et al.*,[30] who extract attached-eddy type modes from the Navier-Stokes equations, suggest that progress in incorporating attached eddies with the equations of motion may be promising. Moreover, Klewicki[31,32] has shown that a self-similar hierarchical structure, which is central to the attached eddy model, is consistent with invariant solutions associated with the leading order mean dynamics. However, we note again that, accounting for dynamical behaviour is beyond the scope of the present work and the Navier-Stokes equations are not used in the model.

In addition to the conditions above, the model is based upon the following assumptions:

1. The flow field is modelled by a hierarchy of eddies, each of which extends from the wall into the flow, and whose dimensions scale with its distance from the wall. These eddies take the form of a spatially bounded structure within the velocity field of the flow.
2. The eddies are geometrically self-similar, having an identical shape regardless of their size (so that the velocity fields corresponding to each are identical once scaled by their heights).
3. The eddies are perfectly randomly placed upon the wall and their locations are entirely independent of each other. Importantly, this means that the eddies are not prevented from overlapping and two or more eddies may occupy the same region of space. (Available spatial datasets of velocity fields from particle-image-velocimetry and direct-numerical simulation indicate that eddies may indeed overlap in this way.[24,33])
4. The total flow field is the sum of the velocity fields corresponding to each individual eddy (plus a potential flow to recover the freestream velocity).

For the mathematical description, we begin by considering $\mathbf{U}_{one\ eddy}(\mathbf{x}-\mathbf{x}_e, h)$, the flow field at $\mathbf{x}$ induced by a representative eddy of height h located at $\mathbf{x}_e = (x_e, y_e, 0)$. An example of the streamwise velocity field associated with one such representative eddy is illustrated in Figure 1. It is noted that such an eddy can correspond to either a single hairpin-type vortex or a "packet" of such vortices (as shown in Figure 1), or other possible physical scenarios. (It is noted that in the following, for the modelling of the velocity statistics, the specification of an "eddy" only requires the specification of the velocity field $\mathbf{U}_{one\ eddy}$.)

As Townsend argued, the flow in the log-region will be inviscid, which implies that the *friction velocity* is the native velocity scale for this system.[2] The native length scale is simply the height of the eddy. It follows from this that the velocity field corresponding to an eddy of any size can be expressed as

$$\mathbf{U}_{one\ eddy} = \mathbf{Q}\left(\frac{\mathbf{x}-\mathbf{x}_e}{h}\right). \tag{4}$$

Note that conventional notation would denote $\mathbf{U}$, as we have defined it here, by $\mathbf{U}^+$ (and this is how it has been denoted in the Introduction). For simplicity, we omit the + notation from here on.

Since the total velocity at any location within the log region will simply be the superposition of the velocities induced by each of the individual eddies, if we knew the locations and heights of

every eddy, the overall flow field would simply be

$$\mathbf{U}(\mathbf{x}) = \sum_k \mathbf{Q}\left(\frac{\mathbf{x} - \mathbf{x}_{e_k}}{h_k}\right), \tag{5}$$

where the $\mathbf{x}_{e_k}$s and h_ks refer to the locations and heights of each individual eddy. Of course, we could never know the locations and heights of every eddy present within the enigmatic chaos of a turbulent flow. We therefore consider only the statistical behaviour of large numbers of such eddies.

When the $\mathbf{x}_{e_k}$s are randomly distributed according to Poisson statistics, the sum in (5) is a generalization of the classical "shot noise" process describing the emission of electrons at random points in time. In the present case, the points are randomly and uniformly distributed over the $(x, y, 0)$ plane.

A. The distribution of eddy sizes

Here, we wish to derive $P(h)$, the probability density function for the height of an eddy. To begin, we note that the velocity fields corresponding to each individual eddy are geometrically identical and unaffected by the presence of nearby eddies. They therefore may each be considered independently. Because each eddy is characterised by its height, all spatial dimensions of the eddy scale with h, and the average volume of space per eddy is therefore proportional to h^3.

$P(h)$ will be proportional to the density of the eddies, where we can define the density as the expected number of eddies, N_e, to be found within a square patch of wall of length and width ℓ, whose heights are between ℓ and $\ell + \mathrm{d}\ell$, divided by this volume. All dimensions of this volume scale with distance from the wall. (It is, of course, required that both ℓ and $\ell + \mathrm{d}\ell$ are between h_{min} and h_{max}.) That is,

$$P(h) \propto \frac{N_e}{\ell^2 \mathrm{d}\ell}. \tag{6}$$

In addition, if we define V_e as the proportion of the volume of a single eddy that is located within $\ell^2 \mathrm{d}\ell$, then

$$N_e = \frac{\ell^2 \mathrm{d}\ell}{V_e}. \tag{7}$$

However, for our geometrically similar eddies, N_e must be invariant for any value of $h \propto \ell$ for any wall-normal position in the log region. To help illustrate this, a schematic is shown in Figure 2 using an analogous discrete system of attached eddies, adapted from Perry and Chong.[17] Here, the volume (represented by the blue rectangles) has dimensions that scale with its distance from the wall, and contains a fixed fraction of eddies within that domain because the eddy heights (and their average spacing in the plane of the wall) also scale with their distance from the wall. This also applies in the continuous case as there is only one length scale. Consequently, for N_e to be invariant for $h \propto \ell$ requires

$$V_e \propto h^3, \tag{8}$$

and therefore, V_e is a fixed fraction of the volume of an individual eddy.

From (6), (7), and (8), we see that the probability density function will be

$$P(h) \propto \frac{1}{h^3}. \tag{9}$$

Since each eddy has a size between h_{min} and h_{max}, we can normalise $P(h)$ to

$$P(h) = 2\left(h_{min}^{-2} - h_{max}^{-2}\right)^{-1} \frac{1}{h^3}. \tag{10}$$

This value of $P(h)$ has been implicitly used in the prior work of Townsend, Perry and Chong, and others. However, until now, this distribution of eddy heights has merely been assumed for convenience. Here, we see that it is in fact mathematically precise for randomly located eddies that are geometrically similar and scale with their distance from the wall. The same result is found to also

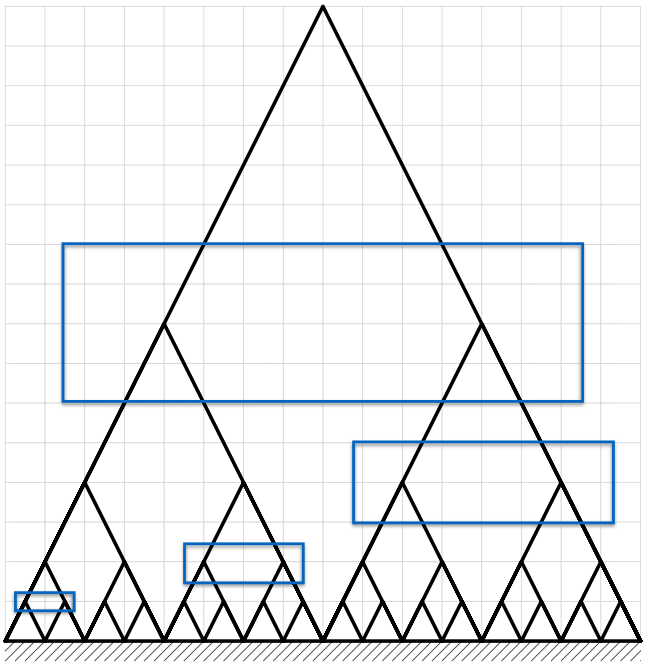

FIG. 2. Symbolic representation for an analogue discrete system of attached eddies. A self-similar pattern is observed for the blue rectangles, which indicate volumes with dimensions that scale with its distance from the wall and contain a fixed fraction of eddies within the domain at all heights.

follow for a discrete distribution of eddy heights, as previously described by Perry and Chong,[17] and this is demonstrated in Appendix A.

B. The statistical properties of the flow and the eddy contribution functions

The attached eddy model has previously been used to derive the mean velocity profile and the second order moments. Here, we place these derivations on a more rigorous mathematical base and extend the derivation to include all higher order moments of the velocity. To do this, we employ Campbell's theorem,[34] which was originally proposed for the study of the statistical properties of thermally agitated electrons, whose times of arrival at an anode are perfectly random. Here, we use Campbell's theorem to study the velocity field corresponding to a forest of eddies that are randomly distributed on a plane. To this end, a proof of the theorem for a randomly distributed forest of eddies of varying heights on a two-dimensional plane is given in Appendix B.

Due to the spatial self-similarity of the eddies, it is convenient to scale all eddies with their heights, and hence we define a height-dependent position vector

$$\mathbf{X} \equiv (X, Y, Z) \stackrel{\text{def}}{=} \frac{\mathbf{x}}{h}. \tag{11}$$

We can now define the eddy contribution functions, $I_{k,l,m}(Z)$, which are integrals over the X-Y plane for $\mathbf{Q}(\mathbf{X})$ and its multiples. They are defined by

$$I_{k,l,m}(Z) \stackrel{\text{def}}{=} \int_{-\infty}^{\infty}\!\!\int Q_x^k(\mathbf{X})\, Q_y^l(\mathbf{X})\, Q_z^m(\mathbf{X})\, \mathrm{d}X\, \mathrm{d}Y, \tag{12}$$

where Q_x, Q_y, and Q_z are the orthogonal components of $\mathbf{Q}$, and k, l, and m are positive integers or zero. These eddy contribution functions are a similar concept to the eddy intensity functions introduced by Townsend.[2] The important differences between the two are that they have been scaled differently, and that Townsend's eddy intensity functions are only defined for second order velocity moments (that is, for where $k + l + m = 2$). Therefore, the functions $I_{2,0,0}$, $I_{0,2,0}$, $I_{0,0,2}$, and $I_{1,1,0}$ in

this work would, respectively, be proportional to the functions I_{11}, I_{22}, I_{33}, and I_{13} as defined on page 153 of Townsend's book.[2]

For convenience, we now define a new set of functions, $\lambda_{k,l,m}$, which we call the cumulants of the velocity:

$$\lambda_{k,l,m}(z) \overset{\text{def}}{=} \beta \int_{h_{min}}^{h_{max}} I_{k,l,m}(Z) h^2 P(h)\, \mathrm{d}h, \tag{13}$$

where β represents the average density per unit area of eddies (of all sizes) at the wall. The eddies have been assumed to range in size from h_{min} to h_{max}. We can therefore associate h_{max} with δ, the boundary layer thickness, which here corresponds to the height of the log region. Hence,

$$h_{max} \propto \delta. \tag{14}$$

It will become necessary subsequently to recognise that β can be related to the number of eddies present, N, and the surface area of the wall they inhabit, L^2, via

$$\beta \equiv \frac{N}{L^2}. \tag{15}$$

Note that we cannot take the $I_{k,l,m}(Z)$ functions outside the integrals in (13), since Z is itself a function of h. These equations have all been derived in the appendix. Since we are most interested in the streamwise velocity, we introduce a shorthand notation for cumulants that only entail streamwise terms

$$\lambda_n \equiv \lambda_{n,0,0}. \tag{16}$$

The derivation in the appendix demonstrates that Campbell's theorem allows the statistical properties of the flow to be determined from the velocity field corresponding to a single representative eddy. This is ultimately because the combined effects of multiple perfectly randomly placed eddies will contribute to the moments of the total velocity, such as $\langle U^2 \rangle$, but not to the moments of the velocity fluctuations, such as $\langle u^2 \rangle$. This can be seen most clearly in the derivation previously presented by the authors.[35] (We must stress that these are not assumptions we have made within the model, but are instead both consequences of the assumptions that have been made at the beginning of this section.)

The mean velocity is given by

$$\langle U \rangle = \lambda_1, \qquad \langle V \rangle = \lambda_{0,1,0}, \qquad \langle W \rangle = \lambda_{0,0,1}. \tag{17}$$

Throughout this work, angled brackets are used to denote ensemble averages. Specifically, these are averages over all of the possible locations of each of the eddies present.

These equations could alternatively be expressed in terms of the velocity field emanating from a single eddy via

$$\langle \mathbf{U} \rangle = \beta \int_{h_{min}}^{h_{max}} P(h) \iint_{-\infty}^{\infty} \mathbf{Q}\left(\frac{\mathbf{x}}{h}\right) \mathrm{d}x\, \mathrm{d}y\, \mathrm{d}h, \tag{18}$$

thus giving an expression for the average velocity of a turbulent flow in terms of the velocity field corresponding to just a single eddy. This is relatively simple to derive since $\mathbf{U}$ is a linear quantity, which can therefore be split into a series of components. Velocity correlations between two or more eddies will therefore not affect $\langle \mathbf{U} \rangle$. The same cannot be said for non-linear quantities, such as the velocity squared or the Reynolds shear stress. It is in order to derive these, and higher order moments of the velocity fluctuations, that we introduce the use of Campbell's theorem to the attached eddy hypothesis in this work.

But first, we must consider non-linear quantities, and how and whether the combined effects of the velocities of two or more eddies may affect such quantities. We define a fluctuating velocity, $\mathbf{u}(\mathbf{x})$ as a deviation away from the mean velocity via

$$\mathbf{u}(\mathbf{x}) = \mathbf{U}(\mathbf{x}) - \langle \mathbf{U}(\mathbf{x}) \rangle. \tag{19}$$

The second order moments of the velocity fluctuations are related to the cumulants via

$$\langle u^2 \rangle = \lambda_2, \qquad \langle v^2 \rangle = \lambda_{0,2,0}, \qquad \langle w^2 \rangle = \lambda_{0,0,2}. \tag{20}$$

We will demonstrate in Sec. III that (17) returns the log-laws of Perry and Chong[17] given in (2) and (20) returns the Townsend[2] relations given in (1). The derivations of the first and second order moments given in (17) and (20) are relatively straightforward, and a derivation has previously been given by Marusic and Woodcock.[35]

In order to derive the higher order moments of the velocity fluctuations, we have introduced a new methodology, which we detail in Appendix B. There is no simple closed form function which relates $\langle u^n \rangle$, $\langle v^n \rangle$, and $\langle w^n \rangle$ to the cumulants for arbitrary n. However, we can derive such relations for any specific n, and the procedure for doing so is described in Appendix B.

The following relations have been derived from Eqs. (B14) and (B16) of the appendix. The higher order powers of the fluctuating velocities relate to these cumulants via

$$\langle u^3 \rangle = \lambda_3, \tag{21a}$$

$$\langle u^4 \rangle = \lambda_4 + 3\lambda_2^2, \tag{21b}$$

$$\langle u^5 \rangle = \lambda_5 + 10\lambda_2\lambda_3, \tag{21c}$$

$$\langle u^6 \rangle = \lambda_6 + 15\lambda_2\lambda_4 + 10\lambda_3^2 + 15\lambda_2^3, \tag{21d}$$

$$\langle u^7 \rangle = \lambda_7 + 21\lambda_2\lambda_5 + 35\lambda_3\lambda_4 + 105\lambda_2^2\lambda_3, \tag{21e}$$

$$\langle u^8 \rangle = \lambda_8 + 28\lambda_2\lambda_6 + 56\lambda_3\lambda_5 + 35\lambda_4^2 + 210\lambda_2^2\lambda_4 + 280\lambda_2\lambda_3^2 + 105\lambda_2^4, \tag{21f}$$

$$\langle u^9 \rangle = \lambda_9 + 36\lambda_2\lambda_7 + 84\lambda_3\lambda_6 + 126\lambda_4\lambda_5 + 378\lambda_2^2\lambda_5 + 1260\lambda_2\lambda_3\lambda_4 + 280\lambda_3^3 + 1260\lambda_2^3\lambda_3, \tag{21g}$$

$$\langle u^{10} \rangle = \lambda_{10} + 45\lambda_2\lambda_8 + 120\lambda_3\lambda_7 + 210\lambda_4\lambda_6 + 630\lambda_2^2\lambda_6 + 126\lambda_5^2 + 2520\lambda_2\lambda_3\lambda_5 + 1575\lambda_2\lambda_4^2 + 2100\lambda_3^2\lambda_4 + 3150\lambda_2^3\lambda_4 + 6300\lambda_2^2\lambda_3^2 + 945\lambda_2^5, \tag{21h}$$

and similarly for $\langle v^n \rangle$ and $\langle w^n \rangle$.

The paradigms for a selected number of cross-correlated averages are

$$\langle uv \rangle = \lambda_{1,1,0}, \tag{22a}$$

$$\langle uw \rangle = \lambda_{1,0,1}, \tag{22b}$$

$$\langle u^2 w \rangle = \lambda_{2,0,1}, \tag{22c}$$

$$\langle u^2 v \rangle = \lambda_{2,1,0}, \tag{22d}$$

$$\langle uvw \rangle = \lambda_{1,1,1}, \tag{22e}$$

$$\langle u^2 v^2 \rangle = \lambda_{2,2,0} + \lambda_{2,0,0}\lambda_{0,2,0} + 2\lambda_{1,1,0}^2, \tag{22f}$$

$$\langle u^2 w^2 \rangle = \lambda_{2,0,2} + \lambda_{2,0,0}\lambda_{0,0,2} + 2\lambda_{1,0,1}^2, \tag{22g}$$

$$\langle u^3 v \rangle = \lambda_{3,1,0} + 3\lambda_{1,1,0}\lambda_{2,0,0}, \tag{22h}$$

$$\langle u^2 vw \rangle = \lambda_{2,1,1} + \lambda_{0,1,1}\lambda_{2,0,0} + 2\lambda_{1,0,1}\lambda_{1,1,0}. \tag{22i}$$

C. Comparison to Gaussian velocity statistics

It has previously been shown that perfectly random eddies will, in the large β limit, approach perfectly Gaussian behaviour,[28] and that their even moments will behave according to

$$\lim_{\beta\to\infty} \langle u^{2p} \rangle^{1/p} = [(2p-1)!!]^{1/p} \langle u^2 \rangle, \tag{23}$$

where $n!! \equiv n(n-2)(n-4)\ldots 1$. It can be shown by inspection that these concur with the results given in (21). This we can easily discern from the fact that every $\lambda_{k,l,m}$ is proportional to β, and so at large β, the right hand side of (21) will always be dominated by the highest powered term. This, for even powers, will always be the term containing only a power of λ_2.

It is clear from (13) that according to this present model, λ_4 must be positive. It follows therefore that the "flatness" (which is defined as $\langle u^4\rangle/\langle u^2\rangle^2$) must be greater than 3. However, a survey of experimental data shows that the flatness in the streamwise direction is in fact less than 3 (this is referred to as sub-Gaussian behaviour[28]). From this, we can only conclude that λ_4 must be negative in real turbulent flows. It is possible that the placement of eddies in real turbulent flows is not perfectly random, and that instead, the locations of nearby eddies will interact nonlinearly. This may explain the sub-Gaussian behaviour of the streamwise velocity fluctuations. This, however, remains speculation and is beyond the scope of this present work.

The spanwise and wall-normal velocity fluctuations, on the other hand, show reliably super-Gaussian behaviour (i.e., their flatness is greater than 3),[36] which is in line with the results of this present model. We will show in Sec. III B that the wall-normal velocity fluctuations will never follow a Gaussian distribution, regardless of the Reynolds number. This results mathematically from the fact that the fluid cannot flow through the wall.

As with all physical models, the attached eddy model is not intended to predict every aspect of real turbulent flows, but only to capture certain flow behaviours. Specifically, this model seeks to capture the statistical behaviour of the inertial scale, energy-containing, motions in the log region. Where models such as these succeed and fail to capture the behaviours of real flows can be instrumental in determining the nature of the flows themselves. The implications of these results will be elaborated upon in Sec. IV.

III. VELOCITY STATISTICS

We may now use the attached eddy model to derive the statistical properties of the flow. If we know the form that the attached eddies will take, then we can derive $\mathbf{Q}(\mathbf{x}/h)$, the velocity field corresponding to a single eddy, and from there we can derive the eddy contribution functions and the cumulants and moments of the velocity. However, it is not necessary to know the exact shape that the eddies will take in order to derive information about the functional form of the moments of the velocity. We begin this analysis, therefore, by deriving as many properties of the flow as possible without reference to the specific shape of the eddy, or its corresponding velocity field $\mathbf{Q}(\mathbf{x}/h)$.

A. General flow properties

We will now demonstrate that various properties of the moments of turbulent flows can be derived from the attached eddy hypothesis without reference to the exact shape of the eddy. To this end, we must first recognise that the velocity field associated with an eddy will be negligible far beyond the height of the eddy. (This is elaborated upon in Appendix C.) In other words,

$$\mathbf{Q}\left(\frac{\mathbf{x}}{h}\right) \approx 0, \qquad \text{for } z > \alpha h \quad (\alpha > 1), \tag{24}$$

where α is a constant which is intended to allow the velocity field corresponding to a particular eddy to extend slightly beyond the height of the eddy. Of course, $\mathbf{Q}(\mathbf{x}/h)$ is a continuous function, and so (24) places restrictions on the shape of $\mathbf{Q}(\mathbf{x}/h)$ at higher values of z/h. Importantly, this means that $\mathbf{Q}$ must begin to decrease at some point as z/h increases. This also strongly suggests that a significant contribution to $\mathbf{U}(\mathbf{x})$ is likely to come from where z/h is closer to zero.

Because $\mathbf{Q}$ is assumed to be non-zero only for $z/\alpha \le h \le h_{max}$, we need not integrate from h_{min} to h_{max} in (13) if $z > \alpha h_{min}$. This is because if $\mathbf{Q}$ is zero at a certain z/h, then from (12), we can see that so too will be $I_{k,l,m}$. Given this, (13) becomes,

$$\lambda_{k,l,m}(z) = \begin{cases} \beta \displaystyle\int_{z/\alpha}^{h_{max}} I_{k,l,m}\left(\frac{z}{h}\right) h^2 P(h)\,\mathrm{d}h, & \text{for } z > \alpha h_{min}, \\ \beta \displaystyle\int_{h_{min}}^{h_{max}} I_{k,l,m}\left(\frac{z}{h}\right) h^2 P(h)\,\mathrm{d}h, & \text{for } z \le \alpha h_{min}. \end{cases} \tag{25}$$

If we take the $z > \alpha h_{min}$ case in the above equation, after substituting (10) for $P(h)$, it can be rearranged using (11) to be

$$\lambda_{k,l,m}(z) = 2\beta\left(h_{min}^{-2} - h_{max}^{-2}\right)^{-1} \int_{z/h_{max}}^{\alpha} I_{k,l,m}(Z)\frac{\mathrm{d}Z}{Z}. \tag{26}$$

(For reference, the integral above is equivalent to the expression adopted by Townsend,[2] on page 154, for $\lambda_{1,0,1}$.)

We can now use this analysis to find the dominant term in each $\lambda_{k,l,m}(z)$. This is the most we can determine about the exact nature of any $\lambda_{k,l,m}(z)$ without an extensive model of $\mathbf{Q}$.

The corollary to (24), and the fact that $I_{k,l,m}$ will diminish at higher Z, is that a significant contribution to $\lambda_{k,l,m}$ will emanate from around $Z \simeq 0$. It is therefore reasonable to expand $I_{k,l,m}(Z)$ in a Taylor series around $Z = 0$. This results in

$$I_{k,l,m}(Z) = I_{k,l,m}(0) + Z\frac{\mathrm{d}I_{k,l,m}(0)}{\mathrm{d}Z} + \frac{Z^2}{2!}\frac{\mathrm{d}^2I_{k,l,m}(0)}{\mathrm{d}Z^2} + \frac{Z^3}{3!}\frac{\mathrm{d}^3I_{k,l,m}(0)}{\mathrm{d}Z^3} + \cdots. \tag{27}$$

Substituting this into (26) and integrating gives

$$\lambda_{k,l,m}(z) = -\frac{2\beta}{h_{min}^{-2} - h_{max}^{-2}}\left[\log\left(\frac{z}{h_{max}}\right)I_{k,l,m}(0) + \frac{z}{h_{max}}\frac{\mathrm{d}I_{k,l,m}(0)}{\mathrm{d}Z} + \frac{1}{2!\,2}\left(\frac{z}{h_{max}}\right)^2\frac{\mathrm{d}^2I_{k,l,m}(0)}{\mathrm{d}Z^2} + \cdots\right] + B_{k,l,m}, \tag{28}$$

where the $B_{k,l,m}$'s denote constants.

If we restrict ourselves to the region in which $z \ll h_{max}$, we can see that it will be the lowest ordered non-zero term in the Taylor series expansion that dominates the sum in (28). The dominant behaviour of $\lambda_{k,l,m}(z)$ will therefore depend on whether $I_{k,l,m}$, and its derivatives, are zero at $z = 0$. It is therefore necessary to explore the nature of $I_{k,l,m}(Z)$ in order to derive the profiles of any moments of the velocity.

Since this model covers only the log-region, it does not extend to the wall. For that reason, the standard no-slip boundary condition does not apply. Instead, following the approach of Townsend,[2] we apply the method of images. This entails pairing each eddy with a corresponding "mirror" eddy beneath the wall, so that the flows above and below the wall will obey

$$(U(x,y,-z),V(x,y,-z),W(x,y,-z)) = (U(x,y,z),V(x,y,z),-W(x,y,z)). \tag{29}$$

This ensures that the flow will not penetrate through the wall. Note too that the average streamwise flow at the wall, from the attached eddies, will be negative. The reason for this is that the velocity field has effectively been derived from the vorticity field via the Biot-Savart integral. This will inevitably overlook a constant of integration,[37] which is the irrotational portion of the flow. In a real turbulent flow, $\langle U\rangle$ would be positive at the boundary between the near-wall viscous region and the log region, and thus, the addition of an irrotational streamwise flow of magnitude U_∞/u_τ is required. The effect of the eddies will then be to reduce the average flow rate against this irrotational flow.

We can see then that the boundary conditions, at $z = 0$, must take the form

$$\langle\mathbf{U}\rangle(0) = (U_0, V_0, 0), \tag{30}$$

where U_0 and V_0 are as yet unknown constants. The wall normal velocity must be universally zero in order to satisfy (29). The wall-normal contribution of a single eddy, Q_z, must also be zero at the wall, because the wall-normal contributions of the eddy and its corresponding mirror eddy must cancel each other out at the wall.

We would naturally expect V_0 to be zero, via symmetry, if the eddies are facing the streamwise direction and are symmetric in the spanwise direction. We would not, however, expect $Q_y(\mathbf{X})$ to be universally zero, even at the wall, since eddying motions must exist in at least two dimensions.

The boundary conditions acting on $\mathbf{Q}(\mathbf{X})$ must therefore take the form

$$\mathbf{Q}(X,Y,0) = (Q_{x,0}(X,Y), Q_{y,0}(X,Y), 0), \tag{31}$$

where $Q_{x,0}(X,Y)$ and $Q_{y,0}(X,Y)$ are functions that will depend on the exact nature and shape of the eddies. We now have enough information to make a general statement about the boundary conditions applying to all of the eddy contribution functions at $Z = 0$. We can determine which of $I_{k,l,m}$ and its derivatives are expected to be zero by inspection of (12).

By taking into account the fact that it is only the wall-normal velocity, w, that is expected to be zero at $z = 0$, we can see that if $\lambda_{k,l,m}$ has no wall-normal dependence (i.e., $m = 0$), it will be dominated by a logarithmic term. Conversely, if $\lambda_{k,l,m}$ has a wall-normal dependence, it will be dominated by a term of order m. If we assume that all terms apart from the dominant term and the constant are small, we can represent this via

$$\lambda_{k,l,m} \approx \begin{cases} -\dfrac{2\beta}{h_{min}^{-2} - h_{max}^{-2}} I_{k,l,m}(0) \log\left(\dfrac{z}{h_{max}}\right) + B_{k,l,m}, & \text{if } m = 0, \\ -\dfrac{2\beta}{h_{min}^{-2} - h_{max}^{-2}} \dfrac{1}{m!\, m} \dfrac{\mathrm{d}^m I_{k,l,m}(0)}{\mathrm{d}Z^m} \left(\dfrac{z}{h_{max}}\right)^m + B_{k,l,m}, & \text{if } m \neq 0. \end{cases} \tag{32}$$

This implies that all moments of the streamwise and spanwise velocities will contain logarithmic terms, while all moments of the wall-normal velocity will have a power-law dependence at sufficiently high Reynolds number. (It should be noted, however, that as we are considering the flow where $z \ll h_{max}$, we would expect the constant $B_{k,l,m}$ to dominate over all powers of z/h_{max}, but not over the logarithmic terms.) It also implies that the mathematical reason why the wall-normal fluctuations follow a power-law, rather than a logarithm, is because the wall-normal flow must be universally zero at $Z = 0$.

These results concur generally with the recent work of Stevens, Wilczek, and Meneveau, who computed the higher order moments, in all three directions, via a large eddy simulation.[38]

One caveat must be made here: as we have stated, if the eddies face the streamwise direction, and are symmetric in the spanwise direction, we would expect that $I_{0,1,0}(0) = 0$. It would be possible (but unlikely) for $I_{k,l,0}(Z)$ to be zero for some other k and l (and similarly for the derivatives of $I_{k,l,m}$). Whether it was zero or not would depend on the shape of the eddy.

Again, we would expect that for streamwise-facing, spanwise-symmetric eddies, $I_{0,1,0} = 0$, and therefore, the spanwise velocity profile, $\langle V \rangle$, will be zero, rather than logarithmic. We must countenance the possibility that some other $I_{k,l,m}$s (or their derivatives) could also be zero.

However, where any of the $I_{k,l,m}$s for $m \neq 0$ are zero, they are so because of the shape of the eddy. The $m = 0$ cases, on the other hand, must be zero because of the impermeability of the wall.

(It should be noted that this does not imply that all moments with wall-normal components will be dominated by a power-law. For example, in Eq. (22), we can see that $\langle u^2 w^2 \rangle$ will have a dependence on $\lambda_{2,0,0}$, which is logarithmic.)

1. Reynolds number dependence

In this work, we define the Reynolds number based upon the range of eddy scales present within the flow

$$Re_\tau = 100 \frac{h_{max}}{h_{min}}. \tag{33}$$

This follows from the classically adopted assumption that the Kline scaling[39] applies, where $h_{min}^+ = 100$. Alternatively, if one adopts $h_{min}^+ = 2.6 Re_\tau^{1/2}$, following Klewicki,[32] the Reynolds number would be

$$Re_\tau = \left(2.6 \frac{h_{max}}{h_{min}}\right)^2. \tag{34}$$

However, the qualitative results using either (33) or (34) throughout this paper would be the same.

Using the Reynolds number defined in (33), we can express the cumulants given in (32) in terms of Re_τ. To do so, we must express β in terms of h_{min} and h_{max}. To this end, we must express N, the number of eddies present, in terms of h_{min} and h_{max}.

Since the placement of the eddies is a Poisson process, we can infer N from the expected distance from a single eddy to its nearest neighbour in the positive x and y directions. The spatial self-similarity of the eddies affects not only their heights and intensities but also the average distances between them. However, it also follows from the fact that the placement of eddies is a Poisson process that the expected distance to each subsequent eddy will depend only on the height of the subsequent eddy (and not the previous eddy).

Hence, we now define a new constant k_x, such that the expected distance to the next-closest eddy in the positive x-direction will always be $k_x h$ if the height of the next-closest eddy was known to be h. (More specifically, $k_x h$ represents the distance in a strip of height h' to the nearest eddy of height between h and $h + \mathrm{d}h$ divided by h' and $\mathrm{d}h$.) For the spanwise direction, we define an analogous constant k_y.

If the nearest eddy in the positive x-direction was known to be of height h_1 and the nearest eddy in the positive y-direction was known to be of size h_2, then we would know that the number of eddies present, on a plane of area L^2, would be expected to be

$$N_{h_1,h_2} = \frac{L^2}{(k_x h_1)(k_y h_2)}. \tag{35}$$

We can now infer N from the probability density of the eddy heights via

$$N = \int_{h_{min}}^{h_{max}} \int N_{h_1,h_2} P(h_1) P(h_2)\, \mathrm{d}h_1\, \mathrm{d}h_2. \tag{36}$$

By substituting (10) into the above, and integrating, we find that

$$N = \frac{4}{9} \frac{L^2}{k_x k_y} \frac{\left(1 - \left(\frac{h_{min}}{h_{max}}\right)^3\right)^2}{h_{min}^2 \left(1 - \left(\frac{h_{min}}{h_{max}}\right)^2\right)^2}. \tag{37}$$

By using the fact that $\beta \equiv N/L^2$, we can rewrite β as

$$\beta = \frac{4}{9} \frac{1}{k_x k_y} \frac{\left(1 - \left(\frac{h_{min}}{h_{max}}\right)^3\right)^2}{h_{min}^2 \left(1 - \left(\frac{h_{min}}{h_{max}}\right)^2\right)^2}. \tag{38}$$

By substituting this β into (32), we can express the cumulants in terms of h_{min} and h_{max}. If we then substitute the Reynolds number for h_{min} and h_{max} using (33), this results in the following for $z \ll h_{max}$:

$$\lambda_{k,l,m} \approx \begin{cases} -\frac{8}{9} \frac{1}{k_x k_y} \frac{\left(1 - 10^6 Re_\tau^{-3}\right)^2}{\left(1 - 10^4 Re_\tau^{-2}\right)^3} I_{k,l,m}(0) \log\left(\frac{z}{h_{max}}\right) + B_{k,l,m}, & \text{if } m = 0, \\ -\frac{8}{9} \frac{1}{k_x k_y} \frac{\left(1 - 10^6 Re_\tau^{-3}\right)^2}{\left(1 - 10^4 Re_\tau^{-2}\right)^3} \frac{1}{m!\, m} \frac{\mathrm{d}^m I_{k,l,m}(0)}{\mathrm{d}Z^m} \left(\frac{z}{h_{max}}\right)^m + B_{k,l,m}, & \text{if } m \neq 0. \end{cases} \tag{39}$$

The cumulants will therefore all display some dependence upon Re_τ, but as we shall subsequently demonstrate in Sec. III B, this Re_τ dependence will rapidly diminish as Re_τ increases.

2. Computed velocity moments

As has been discussed previously in Sec. II B, if the distribution of eddies were perfectly Gaussian, all higher order moments of u could be related to $\langle u^2 \rangle$ via (23). Furthermore, since the eddies have been assumed to be perfectly randomly and independently located in this model, their behaviour must approach Gaussianity as the population of eddies increases. This can be seen easily

in (21), by the fact that every $\lambda_{k,l,m}$ is proportional to β, and hence, in the high β limit, the dominant term in (21) will be the highest powered term.

In order to gain a quantitative approximation for the moments of the velocity, and to determine whether they should be expected to follow a logarithmic profile at higher orders, Biot-Savart computations were carried out for an assumed typical representative eddy shape (together with its image in the wall). The procedure is as described previously by Marusic.[23] The eddy shape chosen is as shown in Figure 1, consisting of a single packet of six arch-shaped vortex rods that are aligned in the streamwise direction in ascending order of height. This arrangement produces long streamwise streaks of high and low streamwise velocity, consistent with previous experimental observations of organised motion in the log layer. The individual arch-shaped vortex rods that form the packet are inclined at an angle of 45° to the wall, and the vorticity within the vortex rods is assumed to decrease exponentially with the distance from the centre of the rod. From the induced velocity field, we are able to estimate the relative magnitudes of the $\lambda_{k,l,m}$s, and thereby determine which terms in (21) can be safely neglected and when.

A comparison of the results obtained for the streamwise velocity moments to their equivalents in a perfectly Gaussian flow are given in Figures 3 and 4(a).

The results in Figure 3 show that even at Reynolds numbers of order 10^9, there remains a noticeable difference between the higher order moments and their Gaussian equivalents. However, Figure 4(a) shows that such differences do not lead to distinguishable departures from a logarithmic curve—while the additive constants in Eq. (3) do change for higher-order moments, any changes in the slopes of the logarithmic formulation are negligible.

For completeness, Figures 4(b) and (c) show comparisons of the Gaussian estimates to the corresponding computed moments for the representative eddy in Figure 1 for the spanwise and wall-normal fluctuating velocities, respectively. Figure 4(d) shows the corresponding computed Reynolds shear stress profile. Like the streamwise moments, the spanwise moments are seen to follow a logarithmic behaviour for all the even high-order moments. The wall-normal moments are also distinctly different from the Gaussian estimates. These differences between the Campbell's and central-limit theorem estimates are further considered in Secs. III C and III D when discussing the skewness and flatness statistics.

It should be noted that if a single arch-shaped vortex were chosen as the representative eddy, rather than the packet of six aligned vortices, a qualitatively similar result is found, albeit with a less pronounced difference from a perfectly Gaussian flow. We emphasise that the results in Figures 3 and 4 are shown to indicate the functional dependencies of the statistics rather than provide quantitative predictions. For that, one would likely require an effective decomposition algorithm

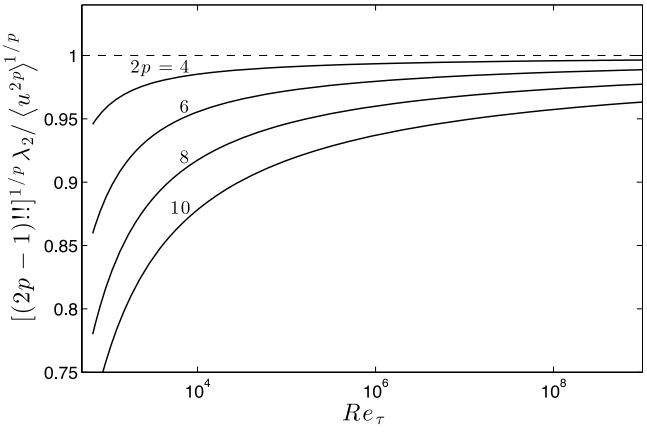

FIG. 3. Plots showing the ratio of the even-numbered higher order moments as derived by Meneveau and Marusic using the central limit theorem to their equivalents derived here via Campbell's theorem, based on the typical attached eddy depicted in Figure 1.[28] Here, $z^+ = 100$, where it is assumed that $Re_\tau = 100h_{max}/h_{min}$.

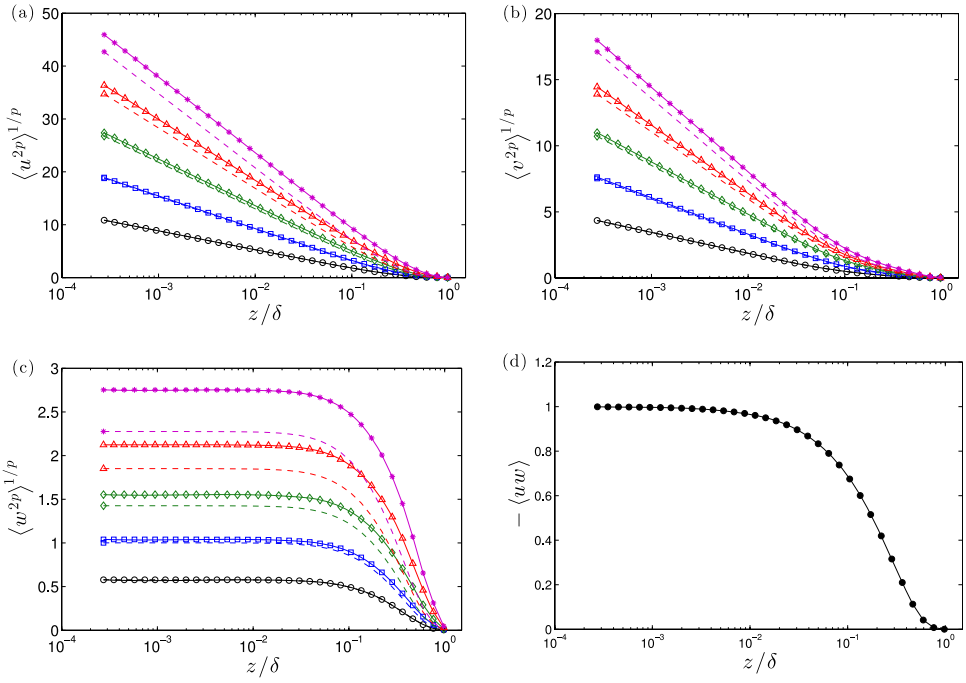

FIG. 4. (a) Computed moments of order $2p = 2$ (○), 4 (□), 6 (◇), 8 (△), and 10 (∗) of streamwise velocity fluctuation as function of wall-normal distance for attached eddy depicted in Figure 1. Solid lines are based on Campbell's theorem (Eq. (21)), and dashed lines are the results due to perfectly Gaussian behaviour (Eq. (23)). (b) and (c), respectively, show corresponding results for spanwise and wall-normal fluctuating velocities. (d) Corresponding Reynolds shear stress.

used with a suitable numerical or experimental database to extract the precise shape and form of the representative eddy structure, and this is beyond the scope of the present study.

B. Implications for the von Kármán constant

We can see from (39) that von Kármán's constant, defined in (2), is given by

$$\frac{1}{\kappa} = -\frac{8}{9}\frac{1}{k_x k_y}\frac{\left(1-10^6 Re_\tau^{-3}\right)^2}{\left(1-10^4 Re_\tau^{-2}\right)^3} I_{1,0,0}(0). \tag{40}$$

This asymptotes to a constant with increasing Re_τ, which we denote by κ_∞. It is given by

$$\kappa_\infty = -\frac{9(k_x k_y)}{8 I_{1,0,0}(0)}. \tag{41}$$

The ratio of von Kármán's constant to its asymptote is given by

$$\frac{\kappa}{\kappa_\infty} = \frac{\left(1-10^4 Re_\tau^{-2}\right)^3}{\left(1-10^6 Re_\tau^{-3}\right)^2}. \tag{42}$$

This variation with Re_τ is plotted in Figure 5. At high Re_τ, (42) asymptotes to

$$\frac{\kappa}{\kappa_\infty} = 1 - 3\times 10^4 Re_\tau^{-2} + O\left(Re_\tau^{-3}\right). \tag{43}$$

Figure 5 also shows the result if Eq. (34) was used to estimate Re_τ.

Townsend[2] (see also Davidson[19]) argued that the magnitude of κ should be expected to change with Reynolds number under the attached eddy hypothesis as the ratio of the energy present in the fluctuations to that present within the mean flow increases. He therefore concluded that any such variations would be unlikely to be detectable under ordinary circumstances, but would become

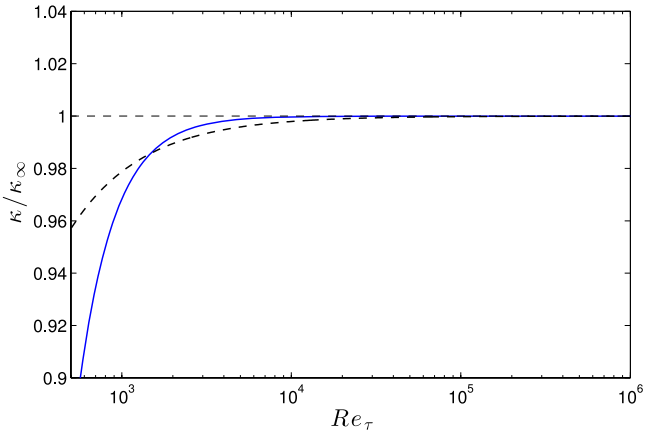

FIG. 5. Von Kármán's constant as a function of Re_τ. Solid and dashed lines correspond to Re_τ based on Eqs. (33) and (34), respectively.

important at extremely large Reynolds numbers. The results here, however, show that while κ does indeed exhibit a small dependence on Re_τ, it rapidly asymptotes to a constant at high Reynolds numbers, provided $h_{max} \gg h_{min}$ (which would be expected for a fully developed turbulent flow). From Figure 5, a negligible variation in κ is seen for $Re_\tau > O(10^4)$.

If $I_{1,0,0}(0)$, k_x, or k_y were different for different wall-bounded flows, then von Kármán's constant would not be universal at high Reynolds numbers. The fact that numerous high Reynolds number experiments[14] support a universal value for κ strongly suggests that k_x, k_y, and $I_{1,0,0}(0)$ are also universal constants (with the latter further suggesting that $I_{1,0,0}(Z)$ is a universal for all Z, meaning that the average shape of the eddies is universal over all smooth walls). Of course, it remains possible that k_x, k_y, and $I_{1,0,0}(0)$ vary, but only in such a way that κ_∞ remains universal. However, that would obviously appear to be an intrinsically less likely explanation.

C. The magnitude and Reynolds number dependence of the skewness

The higher order moments can also be related back to the Reynolds number (and hence the width of the log region). Following the example of Sec. III B, we can use (21) to derive the *skewness* for the streamwise, spanwise, and wall-normal velocities, which we denote by S_u, S_v, and S_w, respectively. The skewness values are given by

$$S_u = \frac{\langle u^3 \rangle}{\langle u^2 \rangle^{3/2}}, \qquad S_v = \frac{\langle v^3 \rangle}{\langle v^2 \rangle^{3/2}}, \qquad S_w = \frac{\langle w^3 \rangle}{\langle w^2 \rangle^{3/2}}. \tag{44}$$

By inspection of (21), we can see that the skewnesses are

$$S_u = \frac{\lambda_3}{\lambda_2^{3/2}}, \qquad S_v = \frac{\lambda_{0,3,0}}{\lambda_{0,2,0}^{3/2}}, \qquad S_w = \frac{\lambda_{0,0,3}}{\lambda_{0,0,2}^{3/2}}. \tag{45}$$

By substituting (39) into the above, we see that the magnitude of S_u decreases gradually with increasing Re_τ due to the logarithmic terms in $\langle u^2 \rangle$ and $\langle u^3 \rangle$. For S_w, we find that

$$S_w = \frac{B_{0,0,3}}{B_{0,0,2}^{3/2}} + O\left(\left(\frac{z}{h_{max}}\right)^2\right) \tag{46}$$

and hence, it rapidly approaches a constant for $z \ll h_{max}$. Again, it must be noted that while (45) coupled with (39) would seem to imply that the spanwise skewness should be non-zero, because the eddies are symmetric in the spanwise direction (except in special circumstances, such as when a cross flow is present), we would expect $I_{0,3,0}$ to be zero, and hence the spanwise skewness to also be zero. It similarly remains perfectly possible for S_u to be zero, under the attached eddy model, even at higher values of z/h_{max}, since $I_3(0)$ may itself be zero or negligible.

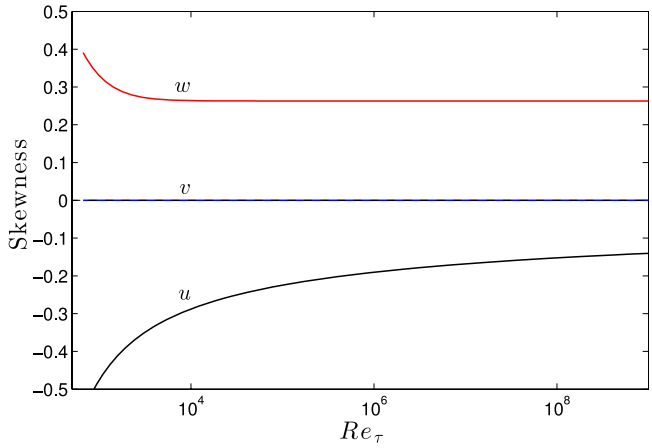

FIG. 6. Plots showing the skewness of the three velocity components calculated using the typical attached eddy depicted in Figure 1 at $z^+ = 100$, where it is assumed that $Re_\tau = 100 h_{max}/h_{min}$.

1. Computed skewness for typical eddy

We also use the Biot-Savart computations introduced in Sec. III A 2, to gain a quantitative appreciation for the magnitude of the skewness. The results can be seen in Figure 6.

The spanwise skewness is, as expected, zero. The streamwise skewness approaches the value of zero with increasing Reynolds number, but again only very slowly. Conversely, the wall-normal skewness much more rapidly approaches a positive value. This all concurs with the analysis of (45).

D. The magnitude and Reynolds number dependence of the flatness

The derivation of the flatness is of particular interest and allows the attached eddy model to be compared qualitatively to experimental results. We denote the flatness, in the streamwise, spanwise, and wall-normal directions by F_u, F_v, and F_w, respectively, where

$$F_u = \frac{\langle u^4 \rangle}{\langle u^2 \rangle^2}, \qquad F_v = \frac{\langle v^4 \rangle}{\langle v^2 \rangle^2}, \qquad F_w = \frac{\langle w^4 \rangle}{\langle w^2 \rangle^2}. \tag{47}$$

Following the example set by the derivation of the skewness, it can be shown that the flatness will be given by

$$F_u = 3 + \frac{\lambda_4}{\lambda_2^2}, \qquad F_v = 3 + \frac{\lambda_{0,4,0}}{\lambda_{0,2,0}^2}, \qquad F_w = 3 + \frac{\lambda_{0,0,4}}{\lambda_{0,0,2}^2}. \tag{48}$$

By substituting (39) into the above, we see that the magnitudes of F_u and F_v approach a value of 3 gradually from above with increasing Re_τ. Conversely, F_w will obey

$$F_w = 3 + \frac{B_{0,0,4}}{B_{0,0,2}^2} + O\left(\left(\frac{z}{h_{max}}\right)^2\right) \tag{49}$$

and so will rapidly approach a constant greater than 3.

If the distribution were perfectly Gaussian, the flatness would be exactly 3. However, from the definition of $\lambda_{k,l,m}$ given in (13), and the definition of $I_{k,l,m}$ given in (12), we can see that λ_4, $\lambda_{0,4,0}$, and $\lambda_{0,0,4}$ must be finite and positive.

According to this present model, therefore, the flatness must be universally super-Gaussian. However, experimental results up to $Re_\tau = 22\,000$ indicate that in the log region $F_u \approx 2.8$, $F_v \approx 3.4$, and $F_w \approx 3.4$.[36] Therefore, the attached eddy results for the spanwise and wall-normal flatnesses qualitatively agree with the observed super-Gaussian behaviour. However, the results for the streamwise component do not, since the experiments have found sub-Gaussian behaviour. This limitation

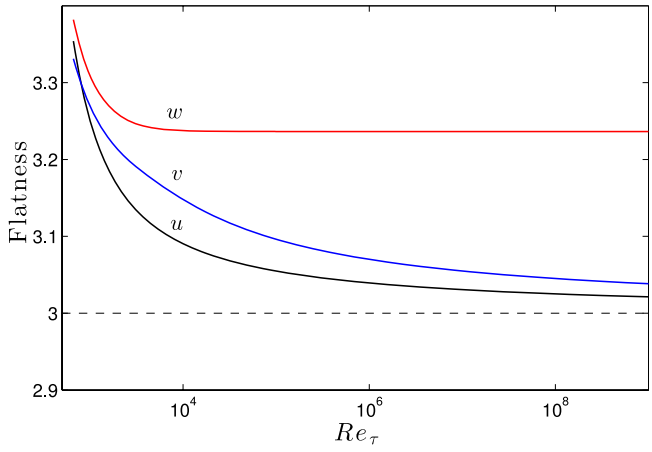

FIG. 7. Plots showing the flatness of the three velocity components calculated using the typical attached eddy depicted in Figure 1 at $z^+ = 100$, where it is assumed that $Re_\tau = 100h_{max}/h_{min}$.

has previously been discussed by Meneveau and Marusic,[28] and requires the model to be modified accordingly.

1. Computed flatness for typical eddy

We obtain a quantitative approximation of the flatness using the Biot-Savart computations introduced in Sec. III A 2. The resulting flatness can be seen in Figure 7.

As we can see, the streamwise and spanwise flatnesses only approach 3 gradually, and remain appreciably greater than 3 at all physically realistic Reynolds numbers. This means, of course, that while the spanwise flatness concurs qualitatively with experimental results, the streamwise flatness remains starkly different. This therefore demonstrates a drawback of the present model and remains the focus of future work.

The wall-normal flatness, by contrast, relatively quickly approaches a value greater than 3. This heavily contrasts with Gaussian behaviour, but agrees qualitatively with experimental results and the observed intermittent nature of the w signal in wall-bounded flows.

IV. CONCLUSIONS

Townsend's attached eddy hypothesis has become a well-known theory for the logarithmic region, where the flow is modelled at the energy-containing scales by a "forest" of self-similar eddies that scale with their distance from the wall and are randomly positioned in the plane of the wall. Using this model, previous studies have been able to derive flow behaviours such as the logarithmic law of the wall and the second-order moments of the velocity fluctuations (1), (2). Here, we revisit the attached eddy model and aim to provide a more rigorous physical and mathematical basis for the analysis, leading to a reduction in the number of heuristic assumptions that were previously used. The new analysis employs an extended version of Campbell's theorem and allows us to use the attached eddy model to derive the moments of the velocity to any order and all cross-correlations between the three velocity components. The results include support for the recent findings of Meneveau and Marusic[28] that all even-ordered moments of the streamwise velocity exhibit a logarithmic dependence on the distance from the wall.

As with earlier applications, our work in effect models the flow via the velocity field associated with a single representative eddy. In order to derive the functional forms of the moments of velocity, it is not necessary to assume the shape of the representative eddy (subject to unknown coefficients). However, the addition of an analysis based upon a typical velocity field for the representative eddy has allowed us to ascertain how similar the flow is to perfectly Gaussian behaviour.

This model predicts that all velocity fluctuations at finite Reynolds number will be super-Gaussian in behaviour (i.e., flatness is greater than 3), with the streamwise and spanwise components approaching Gaussian behaviour asymptotically. The wall-normal fluctuations, however, are shown to remain super-Gaussian at all Reynolds numbers with a positive and finite skewness. (This is a notably different behaviour from that which would be predicted by the use of the central limit theorem, as shown by Meneveau and Marusic.[28]) In the spanwise and wall-normal cases, this agrees with experimental results. Conversely however, experiments have also shown the streamwise fluctuations to be *sub*-Gaussian. This strongly suggests that the coherent structures that form within real turbulent flows may not be distributed perfectly randomly, but instead, their locations will depend in some way upon the locations of nearby eddies. This remains the focus of future work.

This model has also shed light on the nature of von Kármán's constant in the context of the attached eddy hypothesis. There is presently some debate over whether it is truly a constant, or whether it in fact is a function of the flow's properties.[2] We find here that von Kármán's constant does in fact depend very weakly upon the Reynolds number, but that it asymptotes very rapidly to a constant as the Reynolds number increases.

ACKNOWLEDGMENTS

The authors wish to gratefully acknowledge the Australian Research Council for the financial support of this research, and Jason Monty and Charles Meneveau for valuable discussions. We also thank the anonymous reviewers, whose helpful suggestions have improved the manuscript, including the addition of Appendix A.

APPENDIX A: ANALOGUE OF THE EDDY HEIGHT DISTRIBUTION FOR DISCRETE EDDY SIZES

Here, we relate the continuous distribution of eddy heights, $P(h)$, to the equivalent discrete distribution previously employed by Perry and Chong.[17] Perry and Chong elected to employ a distribution in which the height of the eddies doubles at every scale, so that

$$h_n = h_{min}, 2h_{min}, 4h_{min}, 8h_{min}, \ldots, 2^{n-1}h_{min}, \ldots. \tag{A1}$$

This implies that the scale, n, relates to the eddy height via

$$n = 1 + \log_2 \frac{h_n}{h_{min}}. \tag{A2}$$

The range of heights represented by each scale are given by $\Delta h_n = h_{n+1} - h_n$, so that

$$\Delta h_n = h_{min}, 2h_{min}, 4h_{min}, 8h_{min}, \ldots, 2^{n-1}h_{min}, \ldots. \tag{A3}$$

We denote by M_n the number of eddies of scale n that will be attached to a section of the wall of unit area. Since the $(n+1)$th scale is twice the size of the nth scale, and there is no length scale present other than the height of the eddy, it follows that there will be as many eddies of scale $n+1$ on a wall-area of $(2L)^2$ as there are eddies of scale n on a wall-area of L^2. Hence,

$$L^2 M_n = (2L)^2 M_{n+1}. \tag{A4}$$

It follows therefore that

$$M_n \propto 2^{-2n}. \tag{A5}$$

We can therefore represent the distribution of eddies as a function of their heights as $M_n/\Delta h_n$. Combining (A5) and (A3) with (A2) then gives

$$\frac{M_n}{\Delta h_n} \propto h_n^{-3}, \tag{A6}$$

and hence, the h-dependence of the distribution of eddy heights is equivalent to $P(h)$.

APPENDIX B: PROOF OF CAMPBELL'S THEOREM APPLIED TO ATTACHED EDDIES

Since Campbell's theorem is usually applied to systems in which events are randomly placed in time, rather than space as the eddies are here, it is worthwhile to extend the existing proofs to cover spacial rather than temporal averages. This is an extension of a proof of Campbell's theorem by Rice.[40] A more limited proof of Campbell's theorem for attached eddies has been presented in a previous work by Marusic and Woodcock.[35] While that proof only applied to first and second order moments of the velocity, the proof presented here can be used to derive to all moments of the velocity.

Central to the following proof are two physical assumptions we have made about the eddies. The first is the inherently reasonable assumption that there is a limited region of space over which the velocity field corresponding to a single eddy is non-negligible. Mathematically, this manifests as the fact that any integral over the x-y plane of the velocity field corresponding to a single eddy will be equivalent.

We illustrate here, in one dimension: for any function $f(x)$,

$$\int_{-\infty}^{\infty} f(x-a)\,\mathrm{d}a = \int_{-\infty}^{\infty} f(x)\,\mathrm{d}x. \tag{B1}$$

In fact, it is not necessary for the integral to be taken over the entire real line. It is sufficient that the value of $f(x)$ should be zero (or negligible) outside the bounds of integration. In this work, we will always take integrals over the entire x-y plane when using the above equation.

The second assumption we make use of is more controversial, namely, that the locations of each eddy are independent of each other. As has been stated in Sec. II, the angled brackets refer to ensemble averages in this work. Again we demonstrate with a one-dimensional example: if $F(x)$ represents the sum of K copies of the function $f(x)$, each of which is randomly located, so that

$$F(x) = \sum_{k=1}^{K} f(x-a_k), \tag{B2}$$

then, the ensemble average of $F(x)$ will be given by

$$\langle F(x)\rangle = \int_{-\infty}^{\infty} p_1(a_1) \int_{-\infty}^{\infty} p_2(a_2) \ldots \int_{-\infty}^{\infty} p_K(a_K) \sum_{k=1}^{K} f(x-a_k)\,\mathrm{d}a_1\,\mathrm{d}a_2, \ldots,\, \mathrm{d}a_K, \tag{B3}$$

where the $p_k(a_k)$ represents the probability that the kth variable has the value a_k. For each element k of the sum above, it is only the integral over a_k that will be non-zero. This is because, as we have assumed, the location of each eddy is independent of the location of every other eddy. The implication is that the above equation can be simplified to

$$\langle F(x)\rangle = \sum_{k=1}^{K} \int_{-\infty}^{\infty} p_k(a_k) f(x-a_k)\,\mathrm{d}a_k. \tag{B4}$$

Characteristic functions will be used within this proof. We will therefore briefly define characteristic functions and explain their relevant characteristics here. If $f(\alpha)$ is a probability density function, its characteristic function, $F(\gamma)$, will be defined via

$$F(\gamma) = \left\langle e^{i\alpha\gamma}\right\rangle = \int_{-\infty}^{\infty} e^{i\alpha\gamma} f(\alpha)\,\mathrm{d}\alpha. \tag{B5}$$

Characteristic functions have three properties of which we make use. The first of these relates to the average of a sum of independent random variables. If we have such a sum of independent random variables

$$S = \alpha_1 + \alpha_2 + \alpha_3 + \cdots + \alpha_k, \tag{B6}$$

then, the characteristic function of the sum will be given by

$$\left\langle e^{iS\gamma}\right\rangle = \left\langle e^{i\alpha_1\gamma}\right\rangle \left\langle e^{i\alpha_2\gamma}\right\rangle \left\langle e^{i\alpha_3\gamma}\right\rangle \ldots \left\langle e^{i\alpha_k\gamma}\right\rangle. \tag{B7}$$

The second property of characteristic functions we use is that we may obtain $f(\alpha)$ from $F(\gamma)$ via

$$f(\alpha) = \frac{1}{2\pi}\int_{-\infty}^{\infty} e^{-i\alpha\gamma}F(\gamma)\,\mathrm{d}\gamma. \tag{B8}$$

The third property of characteristic functions is that they can easily be used to determine higher order moments, so that the nth moment of α will be given by

$$\langle \alpha^n\rangle = i^{-n}\frac{\mathrm{d}^n}{\mathrm{d}\gamma^n}\left\langle e^{i\alpha\gamma}\right\rangle\Big|_{\gamma=0}. \tag{B9}$$

(The subscript $\gamma = 0$ on the right above indicates that γ should be set to zero after all of the indicated differential operations have been performed.) Since we wish to derive $\langle U^k V^l W^m\rangle$, we define a vector $\boldsymbol{\gamma} \equiv (\gamma_x, \gamma_y, \gamma_z)$. We can then define the general higher order moments of the velocity via

$$\left\langle U^k V^l W^m\right\rangle = i^{-(k+l+m)}\frac{\partial^k}{\partial\gamma_x^k}\frac{\partial^l}{\partial\gamma_y^l}\frac{\partial^m}{\partial\gamma_z^m}\left\langle e^{i\mathbf{U}\cdot\boldsymbol{\gamma}}\right\rangle\Big|_{\boldsymbol{\gamma}=\mathbf{0}}. \tag{B10}$$

Alternatively, expanding the integrand in a Taylor series allows the characteristic function to be expressed as

$$\left\langle e^{i\mathbf{U}\cdot\boldsymbol{\gamma}}\right\rangle = \sum_{k=0}^{\infty}\sum_{l=0}^{\infty}\sum_{m=0}^{\infty}\frac{(i\gamma_x)^k}{k!}\frac{(i\gamma_y)^l}{l!}\frac{(i\gamma_z)^m}{m!}\left\langle U^k V^l W^m\right\rangle. \tag{B11}$$

We similarly expand the logarithm of the characteristic function, so that

$$\log_e\left\langle e^{i\mathbf{U}\cdot\boldsymbol{\gamma}}\right\rangle = \sum_{k=0}^{\infty}\sum_{l=0}^{\infty}\sum_{m=0}^{\infty}\frac{(i\gamma_x)^k}{k!}\frac{(i\gamma_y)^l}{l!}\frac{(i\gamma_z)^m}{m!}\lambda_{k,l,m}, \tag{B12}$$

where the $\lambda_{k,l,m}$ are functions to be determined, except that it is understood that

$$\lambda_{0,0,0} = 0, \qquad \text{since } \log_e(1) = 0. \tag{B13}$$

We will subsequently show how these $\lambda_{k,l,m}$s relate to the moments of the velocity fluctuations and the eddy contribution functions. But right now, we can relate these $\lambda_{k,l,m}$s to the moments of $\mathbf{U}$ through a little algebra. From the definition of the $\lambda_{k,l,m}$s, we can see that they will be given by

$$\lambda_{k,l,m} = i^{-(k+l+m)}\frac{\partial^k}{\partial\gamma_x^k}\frac{\partial^l}{\partial\gamma_y^l}\frac{\partial^m}{\partial\gamma_z^m}\log_e\left\langle e^{i\mathbf{U}\cdot\boldsymbol{\gamma}}\right\rangle\Big|_{\boldsymbol{\gamma}=\mathbf{0}}. \tag{B14}$$

It is possible to convert the above into a closed form expression for $\lambda_{k,l,m}$ using Faà di Bruno's formula, but it is quite cumbersome, and less practical than (B14). Especially, as we are unlikely to require moments of much higher order than 10. It is easy to verify from the above equation that

$$\lambda_1 \equiv \lambda_{1,0,0} = \langle U\rangle, \quad \lambda_{0,1,0} = \langle V\rangle, \quad \lambda_{0,0,1} = \langle W\rangle. \tag{B15}$$

It is convenient to note that so long as $k + l + m \geq 2$, $\mathbf{U}$ can be replaced by $\mathbf{u}$ on the right hand side of (B14), without altering the value of $\lambda_{k,l,m}$. Therefore, so long as $k + l + m \geq 2$, we can alternatively write

$$\lambda_{k,l,m} = i^{-(k+l+m)}\frac{\partial^k}{\partial\gamma_x^k}\frac{\partial^l}{\partial\gamma_y^l}\frac{\partial^m}{\partial\gamma_z^m}\log_e\left\langle e^{i\mathbf{u}\cdot\boldsymbol{\gamma}}\right\rangle\Big|_{\boldsymbol{\gamma}=\mathbf{0}}, \tag{B16}$$

which dramatically simplifies the derivation of the moments of $\mathbf{u}$. Using (B16), it is now possible to derive expressions for all moments of the velocity fluctuations. Some of these are given in (21).

In order to complete the proof, we must now show that the $\lambda_{k,l,m}$s given in (B12) relate to the eddy contribution functions via

$$\lambda_{k,l,m} = \beta \int_{h_{min}}^{h_{max}} I_{k,l,m}(Z) h^2 P(h)\, \mathrm{d}h. \tag{B17}$$

We start by recognising that the probability that the velocity, $\mathbf{U}(\mathbf{x})$, is within the range $(\mathbf{U}(\mathbf{x}), \mathbf{U}(\mathbf{x}) + \mathrm{d}\mathbf{U}(\mathbf{x}))$ can be expressed as

$$\sum_{N=0}^{\infty} \Pr\{\text{There are exactly } N \text{ eddies}\} \times \Pr\{\text{Given that there are } N \text{ eddies, } \mathbf{U} \text{ lies in } (\mathbf{U}, \mathbf{U} + \mathrm{d}\mathbf{U})\}. \tag{B18}$$

We now introduce a new probability function, $\Phi(\mathbf{U})$, which represents the probability that the velocity has a particular value. We also introduce the function, $\Phi_N(\mathbf{U})$, which is the probability that $\mathbf{U}$ has a particular value given that there are N eddies. These two functions are related via

$$\Phi(\mathbf{U}) = \sum_{N=0}^{\infty} \mathcal{P}(N) \Phi_N(\mathbf{U}), \tag{B19}$$

where $\mathcal{P}(N)$ represents the probability that there are exactly N eddies. According to Poisson's law of small probabilities, the probability that there will be exactly N eddies on a plane of area L^2 will be

$$\mathcal{P}(N) = \frac{(\beta L^2)^N}{N!} e^{-\beta L^2}. \tag{B20}$$

If we assume that the system contains exactly N eddies, then the characteristic function for the mean velocity will be given by

$$\left\langle e^{i\mathbf{U}_N \cdot \boldsymbol{\gamma}} \right\rangle \equiv \int_{-\infty}^{\infty}\int\int e^{i\mathbf{U}_N \cdot \boldsymbol{\gamma}} \Phi_N(\mathbf{U}_N)\, \mathrm{d}\mathbf{U}_N. \tag{B21}$$

The velocity field that corresponds to these N eddies is given by

$$\mathbf{U}_N(\mathbf{x}) = \sum_{k=1}^{N} \mathbf{Q}\left(\frac{\mathbf{x} - \mathbf{x}_{e_k}}{h_k}\right). \tag{B22}$$

When we take the ensemble average of $\mathbf{U}_N(\mathbf{x})$, we are averaging over infinitely many realisations in which N eddies are randomly placed on a plane of area L^2. The probability density function for perfectly randomly placed eddies is

$$p(\mathbf{x}_e) = \frac{1}{L^2}. \tag{B23}$$

We now wish to determine $\left\langle e^{i\mathbf{U}_{one\ eddy} \cdot \boldsymbol{\gamma}} \right\rangle$, but we do not know the form of $\Phi_{one\ eddy}(U)$, the probability density function for the velocity field corresponding to a single eddy. We therefore instead use the probabilities relating to the locations and heights of the eddies. Hence, using (B23), we can show that the characteristic function of a single eddy will be

$$\begin{aligned}\left\langle e^{i\mathbf{U}_{one\ eddy} \cdot \boldsymbol{\gamma}} \right\rangle &= \int_{-L/2}^{L/2}\int\int \int_{h_{min}}^{h_{max}} \exp\left(i\mathbf{Q}\left(\frac{\mathbf{x} - \mathbf{x}_e}{h}\right) \cdot \boldsymbol{\gamma}\right) P(h)\, \mathrm{d}h\, p(\mathbf{x}_e)\, \mathrm{d}\mathbf{x}_e \\ &= \frac{1}{L^2} \int_{-L/2}^{L/2}\int\int \int_{h_{min}}^{h_{max}} \exp\left(i\mathbf{Q}\left(\frac{\mathbf{x} - \mathbf{x}_e}{h}\right) \cdot \boldsymbol{\gamma}\right) P(h)\, \mathrm{d}h\, \mathrm{d}\mathbf{x}_e. \end{aligned} \tag{B24}$$

Because the right hand side of the above equation contains an integral over the entire x-y plane, we can therefore employ (B1) to simplify it to

$$\left\langle e^{i\mathbf{U}_{one\ eddy}\cdot\boldsymbol{\gamma}}\right\rangle = \frac{1}{L^2}\int_{-L/2}^{L/2}\int_{-L/2}^{L/2}\int_{h_{min}}^{h_{max}} \exp\left(i\mathbf{Q}\left(\frac{\mathbf{x}}{h}\right)\cdot\boldsymbol{\gamma}\right) P(h)\,\mathrm{d}h\,\mathrm{d}x\,\mathrm{d}y, \tag{B25}$$

which importantly means that the characteristic functions of each $\Phi_{one\ eddy}(\mathbf{U},h)$ are identical, regardless of the location of the eddy. By combining (B7) and (B8) with (B22), we find that

$$\Phi_N(\mathbf{U}) = \frac{1}{2\pi}\int_{-\infty}^{\infty}\int_{-\infty}^{\infty}\int_{-\infty}^{\infty} e^{-i\mathbf{U}\cdot\boldsymbol{\gamma}}\left(\frac{1}{L^2}\int_{-L/2}^{L/2}\int_{-L/2}^{L/2}\int_{h_{min}}^{h_{max}} \exp\left(i\mathbf{Q}\left(\frac{\mathbf{x}}{h}\right)\cdot\boldsymbol{\gamma}\right) P(h)\,\mathrm{d}h\,\mathrm{d}x\,\mathrm{d}y\right)^N \mathrm{d}\boldsymbol{\gamma}. \tag{B26}$$

By summing over all N using (B19) and (B20), we can determine the overall probability, $\Phi(\mathbf{U})$. Taking into account the fact that $\mathbf{U}=\mathbf{0}$ for $N=0$, the overall probability can be shown to be

$$\Phi(\mathbf{U}) = \lim_{L\to\infty}\frac{1}{2\pi}\int_{-\infty}^{\infty}\int_{-\infty}^{\infty}\int_{-\infty}^{\infty} \exp\left[-i\mathbf{U}\cdot\boldsymbol{\gamma} - \beta L^2 + \beta\int_{-L/2}^{L/2}\int_{-L/2}^{L/2}\int_{h_{min}}^{h_{max}} \exp\left(i\mathbf{Q}\left(\frac{\mathbf{x}}{h}\right)\cdot\boldsymbol{\gamma}\right)\right.$$
$$\left.\times\, P(h)\,\mathrm{d}h\,\mathrm{d}x\,\mathrm{d}y\right]\mathrm{d}\boldsymbol{\gamma}. \tag{B27}$$

By making use of the fact that

$$\beta L^2 = \beta\int_{-L/2}^{L/2}\int_{-L/2}^{L/2}\int_{h_{min}}^{h_{max}} P(h)\,\mathrm{d}h\,\mathrm{d}x\,\mathrm{d}y, \tag{B28}$$

and taking the limit as $L\to\infty$, (B27) becomes

$$\Phi(\mathbf{U}) = \frac{1}{2\pi}\int_{-\infty}^{\infty}\int_{-\infty}^{\infty}\int_{-\infty}^{\infty} \exp\left\{-i\mathbf{U}\cdot\boldsymbol{\gamma} + \beta\int_{-\infty}^{\infty}\int_{-\infty}^{\infty}\int_{h_{min}}^{h_{max}}\left[\exp\left(i\mathbf{Q}\left(\frac{\mathbf{x}}{h}\right)\cdot\boldsymbol{\gamma}\right) - 1\right] P(h)\,\mathrm{d}h\,\mathrm{d}x\,\mathrm{d}y\right\}\mathrm{d}\boldsymbol{\gamma}. \tag{B29}$$

The characteristic function of a system containing an unspecified number of eddies will be

$$\left\langle e^{i\mathbf{U}\cdot\boldsymbol{\gamma}}\right\rangle \equiv \int_{-\infty}^{\infty}\int_{-\infty}^{\infty}\int_{-\infty}^{\infty} e^{i\mathbf{U}\cdot\boldsymbol{\gamma}}\Phi(\mathbf{U})\,\mathrm{d}\mathbf{U}. \tag{B30}$$

By taking into account the fact that

$$\frac{1}{2\pi}\int_{-\infty}^{\infty}\int_{-\infty}^{\infty}\int_{-\infty}^{\infty} e^{i\mathbf{U}\cdot(\boldsymbol{\gamma}-\boldsymbol{\gamma}')}\,\mathrm{d}\mathbf{U} = \delta_d(\boldsymbol{\gamma}-\boldsymbol{\gamma}'), \tag{B31}$$

where $\delta_d(\boldsymbol{\gamma})$ is a Dirac delta function, the logarithm of the characteristic function can be shown to be

$$\log_e\left\langle e^{i\mathbf{U}\cdot\boldsymbol{\gamma}}\right\rangle = \beta\int_{-\infty}^{\infty}\int_{-\infty}^{\infty}\int_{h_{min}}^{h_{max}}\left[\exp\left(i\mathbf{Q}\left(\frac{\mathbf{x}}{h}\right)\cdot\boldsymbol{\gamma}\right) - 1\right] P(h)\,\mathrm{d}h\,\mathrm{d}x\,\mathrm{d}y, \tag{B32}$$

which, when expanded in a Taylor series becomes

$$\log_e\left\langle e^{i\mathbf{U}\cdot\boldsymbol{\gamma}}\right\rangle = \beta\sum_{k=0}^{\infty}\sum_{l=0}^{\infty}\sum_{m=0}^{\infty}\frac{(i\gamma_x)^k}{k!}\frac{(i\gamma_y)^l}{l!}\frac{(i\gamma_z)^m}{m!}$$
$$\times\int_{-\infty}^{\infty}\int_{-\infty}^{\infty}\int_{h_{min}}^{h_{max}}\left[Q_x^k\left(\frac{\mathbf{x}}{h}\right)Q_y^l\left(\frac{\mathbf{x}}{h}\right)Q_z^m\left(\frac{\mathbf{x}}{h}\right) - 1\right] P(h)\,\mathrm{d}h\,\mathrm{d}x\,\mathrm{d}y. \tag{B33}$$

By equating the coefficients above with those in (B12), we find that the $\lambda_{k,l,m}$s are given by

$$\lambda_{k,l,m} = \beta \int_{-\infty}^{\infty}\int_{-\infty}^{\infty}\int_{h_{min}}^{h_{max}} Q_x^k\left(\frac{\mathbf{x}}{h}\right) Q_y^l\left(\frac{\mathbf{x}}{h}\right) Q_z^m\left(\frac{\mathbf{x}}{h}\right) P(h)\,\mathrm{d}h\,\mathrm{d}x\,\mathrm{d}y, \tag{B34}$$

which satisfies (B17) and thereby concludes the proof.

APPENDIX C: IMPLICATIONS OF BIOT-SAVART'S LAW

The derivation of the log law given in Sec. III A relies on the statement, given mathematically in (24), that there exists a point above the eddy beyond which the eddy has no significant effect on the flow field. This follows from the Biot-Savart equation on condition that the vorticity field is spatially bounded. This equation states that if $\boldsymbol{\omega}(\mathbf{X})$ is the vorticity field associated with a single eddy, then the velocity field associated with that eddy will be

$$\mathbf{Q}(\mathbf{X}) = \frac{1}{2\pi}\iiint_{\mathcal{V}} \frac{\boldsymbol{\omega}(\mathbf{X}')\times(\mathbf{X}-\mathbf{X}')}{|\mathbf{X}-\mathbf{X}'|^3}\mathrm{d}\mathbf{X}', \tag{C1}$$

where the integral is understood to be evaluated over the entire volume. This implies that at a sufficient distance from the wall,

$$\mathbf{Q}(\mathbf{X}) \sim O\left(\frac{1}{Z^2}\right). \tag{C2}$$

We can therefore infer that as Z increases, $\mathbf{Q}(\mathbf{X})$ will eventually become negligible. This can reasonably be simplified to (24).

[1] A. A. Townsend, "Equilibrium layers and wall turbulence," J. Fluid Mech. **11**, 97–120 (1961).
[2] A. A. Townsend, *The Structure of Turbulent Shear Flow* (Cambridge University Press, 1976).
[3] S. B. Pope, *Turbulent Flows* (Cambridge University Press, 2000).
[4] K. Hanjalić and B. E. Launder, "Contribution towards a Reynolds-stress closure for low-Reynolds-number turbulence," J. Fluid Mech. **74**(4), 593–610 (1976).
[5] R. J. Adrian and I. Marusic, "Coherent structures in flow over hydraulic engineering surfaces," J. Hydraul. Res. **50**, 451–464 (2012).
[6] I. Marusic, B. J. McKeon, P. A. Monkewitz, H. M. Nagib, and A. J. Smits, "Wall-bounded turbulent flows at high Reynolds numbers: Recent advances and key issues," Phys. Fluids **22**, 065103 (2010).
[7] A. J. Smits, B. J. McKeon, and I. Marusic, "High Reynolds number wall turbulence," Annu. Rev. Fluid Mech. **43**, 353–375 (2011).
[8] J. Jiménez, "Cascades in wall-bounded turbulence," Annu. Rev. Fluid Mech. **44**, 27–45 (2012).
[9] J. Jiménez, "Near-wall turbulence," Phys. Fluids **25**, 101302 (2013).
[10] T. B. Nickels, I. Marusic, S. Hafez, N. Hutchins, and M. S. Chong, "Some predictions of the attached eddy model for a high Reynolds number boundary layer," Philos. Trans. R. Soc., A **365**, 807–822 (2007).
[11] G. J. Kunkel and I. Marusic, "Study of the near-wall-turbulent region of the high-Reynolds-number boundary layer using an atmospheric flow," J. Fluid Mech. **548**, 375–402 (2006).
[12] M. Hultmark, M. Vallikivi, S. C. C. Bailey, and A. J. Smits, "Turbulent pipe flow at extreme Reynolds numbers," Phys. Rev. Lett. **108**, 094501 (2012).
[13] R. J. Etter, J. M. Cutbirth, S. L. Ceccio, D. R. Dowling, and M. Perlin, "High Reynolds number experimentation in the US Navy's William B. Morgan large cavitation channel," Meas. Sci. Technol. **16**, 1701–1709 (2005).
[14] I. Marusic, J. P. Monty, M. Hultmark, and A. J. Smits, "On the logarithmic region in wall turbulence," J. Fluid Mech. **716**, R3 (2013).
[15] P. Vincenti, J. C. Klewicki, C. Morrill-Winter, C. M. White, and M. Wosnik, "Streamwise velocity statistics in turbulent boundary layers that spatially develop to high Reynolds number," Exp. Fluids **54**, 1–13 (2013).
[16] J. A. Sillero, J. Jiménez, and R. D. Moser, "One-point statistics for turbulent wall-bounded flows at Reynolds numbers up to $\delta^+ \approx 2000$," Phys. Fluids **25**, 105102 (2013).
[17] A. E. Perry and M. S. Chong, "On the mechanism of wall turbulence," J. Fluid Mech. **119**, 173–217 (1982).
[18] A. E. Perry, S. Henbest, and M. S. Chong, "A theoretical and experimental study of wall turbulence," J. Fluid Mech. **165**, 163–199 (1986).
[19] P. A. Davidson, *Turbulence: An Introduction for Scientists and Engineers* (Oxford University Press, 2004).
[20] A. E. Perry, I. Marusic, and J. D. Li, "Wall turbulence closure based on classical similarity laws and the attached eddy hypothesis," Phys. Fluids **6**(2), 1024–1035 (1994).
[21] A. E. Perry and I. Marusic, "A wall-wake model for the turbulence structure of boundary layers. Part 1. Extension of the attached eddy hypothesis," J. Fluid Mech. **298**, 361–388 (1995).

[22] I. Marusic and A. E. Perry, "A wall wake model for the turbulent structure of boundary layers. Part 2. Further experimental support," J. Fluid Mech. **298**, 389–407 (1995).
[23] I. Marusic, "On the role of large-scale structures in wall turbulence," Phys. Fluids **13**, 735–743 (2001).
[24] R. J. Adrian, C. D. Meinhart, and C. D. Tomkins, "Vortex organization in the outer region of the turbulent boundary layer," J. Fluid Mech. **422**, 1–53 (2000).
[25] N. Hutchins, W. T. Hambleton, and I. Marusic, "Inclined cross-stream stereo PIV measurements in turbulent boundary layers," J. Fluid Mech. **541**, 21–54 (2005).
[26] N. Hutchins and I. Marusic, "Evidence of very long meandering structures in the logarithmic region of turbulent boundary layers," J. Fluid Mech. **579**, 1–28 (2007).
[27] S. Tardu, *Statistical Approach to Wall Turbulence* (Wiley & Sons, 2011).
[28] C. Meneveau and I. Marusic, "Generalized logarithmic law for high-order moments in turbulent boundary layers," J. Fluid Mech. **719**, R1 (2013).
[29] A. S. Sharma and B. J. McKeon, "On coherent structure in wall turbulence," J. Fluid Mech. **728**, 196–238 (2013).
[30] R. Moarref, A. S. Sharma, J. A. Tropp, and B. J. McKeon, "Model-based scaling of the stremwise energy density in high-Reynolds-number turbulent channels," J. Fluid Mech. **734**, 275–316 (2013).
[31] J. C. Klewicki, "A description of turbulent wall-flow vorticity consistent with mean dynamics," J. Fluid Mech. **737**, 176–204 (2013).
[32] J. C. Klewicki, "Self-similar mean dynamics in turbulent wall flows," J. Fluid Mech. **718**, 596–621 (2013).
[33] C. M. de Silva, E. P. Gnanamanickam, C. Atkinson, N. A. Buchmann, N. Hutchins, J. Soria, and I. Marusic, "High spatial range velocity measurements in a high Reynolds number turbulent boundary layer," Phys. Fluids **26**, 025117 (2014).
[34] N. Campbell, "The study of discontinuous phenomena," Proc. Cambridge Philos. Soc. **15**, 117–136 (1909).
[35] I. Marusic and J. D. Woodcock, in *Progress in Wall Turbulence: Understanding and Modelling*, edited by M. Stanislas, J. Jimenez, and I. Marusic (Springer, Dordrecht, 2015), pp. 1–14.
[36] H. H. Fernholz and P. J. Finley, "The incompressible zero-pressure-gradient turbulent boundary layer: An assessment of the data," Prog. Aerospace Sci. **32**, 245–267 (1996).
[37] P. G. Saffman, *Vorticity Dynamics* (Cambridge University Press, 1995).
[38] R. J. A. M. Stevens, M. Wilczek, and C. Meneveau, "Large-eddy simulation study of the logarithmic law for high-order moments in turbulent boundary layers," J. Fluid Mech. **757**, 888–907 (2014).
[39] S. J. Kline, W. C. Reynolds, F. A. Schrab, and P. W. Runstadler, "The structure of turbulent boundary layers," J. Fluid Mech. **30**, 741–773 (1967).
[40] S. O. Rice, "Mathematical analysis of random noise," Bell Syst. Tech. J. **23**, 282–332 (1944).
[41] R. J. Adrian, private communication, 2001.